Effect of uniaxial stress on the fluorine-transferred hyperfine parameters and lattice distortions in alkaline-earth fluorides with Tm^{2+} impurities

C. Fainstein, M. Tovar,* and C. Ramos*
Centro Atómico Bariloche,† and Instituto Balseiro,‡ 8400-Bariloche, Argentina
(Received 27 August 1981)

We have measured the effect of uniaxial stress on the fluorine-transferred hyperfine interaction for Tm^{2+}:CaF_2 and Tm^{2+}:SrF_2 using electron-nuclear double-resonance (ENDOR) techniques. We obtain for $\partial(A_s - A_p)/\partial P$ the values 4.3(4) kHz kg^{-1} mm^2 and 4.2(3) kHz kg^{-1} mm^2, respectively. These results, as well as those obtained for the same hosts without applied stress, are discussed within the framework of an improved model on the lattice distortions around the impurity and its change with uniaxial stress. The positive conclusion of this work is the remarkable agreement between the local distortion predicted by the model and that derived from ENDOR experiments. The same agreement is also found for Eu^{2+} in the fluorides as compared with data derived from measurements of the crystal field. Differences between the experimental data on the stressed samples and the predictions of the model are attributed to stress-induced electric dipoles. We suggest that present uncertainties in the estimate of this contribution can be partially solved by further experiments on trivalent rare-earth metals in the fluorides.

I. INTRODUCTION

The interaction of dilute paramagnetic ions with the crystal-field components induced by local strains of the host lattice is described by the spin-lattice Hamiltonian, a model Hamiltonian whose coefficients are obtained experimentally in terms of macroscopic strains of the host, by measuring the effect of external uniaxial stress on the electron paramagnetic resonance (EPR) spectra of the system.[1] These experiments allow a modification of the crystal field acting on the impurity ion by changing both its symmetry and magnitude. The results thus obtained are of special interest because microscopic theories on electrostatic and covalent bonding can be tested.

Divalent thulium impurities in alkaline-earth fluorides is one of the simplest systems available to test the validity of these theories and for which there is a fair amount of reliable experimental data. Baker and co-workers[2,3] have found an excellent correlation between the spin-lattice relaxation rates measured by Sabisky and Anderson,[4] and those calculated using the results of their EPR and uniaxial stress experiments. Their attempt to interpret the measured spin-lattice parameters in terms of electrostatic and covalent contributions showed the importance of determining the actual equilibrium positions of the impurity neighbors, and also the relation between the stress-induced displacements of the ligands and the macroscopic strain of the host. These "local distortions" are due to the different (as compared with the host) force constants associated with the impurity-ligand interaction, and they have been calculated by Malkin and co-workers[5,6] for rare-earth impurities in fluorite crystals by minimizing the cohesion energy of the impure lattice.

The local distortion is important not only in calculating crystal-field parameters, but also in evaluating the transferred hyperfine interaction of the impurity with the nearest fluorine ions. A remarkable correlation was found by Anderson *et al.*[7] between both sets of parameters for particular values of the $Tm^{2+} \rightarrow F^-$ distance in each of the hosts CaF_2, SrF_2, and BaF_2. These values were obtained from ligand-ENDOR (electron-nuclear double-resonance) data by assuming a direct proportionality between the different covalent contributions to the transferred hyperfine parameters.

The local distortions obtained in this way do not entirely agree with the results of Malkin *et al.*,[6] in particular for CaF_2, where they predict a contraction of the host around the impurity while ENDOR data show an expansion.

Ligand-ENDOR experiments under uniaxial stress provide direct information on the change of the impurity-ligand distance with stress. Baker

and Fainstein[3] attempted to determine the stress dependence of the equilibrium position of the nearest neighbors of Tm^{2+} ions in BaF_2 by measuring the frequency shift of the ligand-ENDOR spectral lines. Their results, compared with predictions based on available theoretical models, showed the necessity of more experimental evidence in order to achieve a better understanding of the local distortion.

In this work we report the extension of those measurements[8] to Tm^{2+}:CaF_2 and Tm^{2+}:SrF_2 as described in Sec. II, where we also analyze the results obtained for the three lattices (including BaF_2) in terms of the local distortion and the changes induced by the applied stress.

In order to obtain a coherent description of the effects described before, we found that it was necessary to improve the model used to calculate both the impurity-ligand distance and its change with applied stress. This was accomplished within the framework of a shell model as described in Sec. III.

II. ENDOR EXPERIMENT

A. Experimental techniques

Single crystals of CaF_2 and SrF_2 nominally doped with 0.05% TmF_3 were purchased from Optovac, Inc. The thulium impurities replace the metal ion and were reduced to the divalent state by electron bombardent ($\sim$1 MeV) in our LINAC facility which has adequate conversion efficiency for our EPR-ENDOR experiments with a 10-min irradiation time. The samples for the stress experiments were prepared by cutting the crystals in the shape of rectangular prisms of about 2-mm length and 1-mm^2 cross section, with their bases being cleavage planes (111). The samples were mounted in the resonator with their axes perpendicular to the plane of rotation of the external magnetic field.

All data were taken at liquid-helium temperatures with an EPR-ENDOR spectrometer, operating at 35 GHz and tunable either to the absorption or dispersion modes. A specially designed TE_{011} cylindrical cavity[9] allows for the application of uniaxial stress perpendicular to the magnetic field. The EPR spectra were obtained using 100-kHz modulation of the magnetic field and phase-sensitive detection. The ENDOR signals were detected through frequency modulation (240 Hz) of the rf field, which was slowly swept through resonance. The ENDOR frequency was accurately measured by simultaneously displaying, in a two-channel recorder, the spectral line and 10-kHz marks obtained from the rf sweeper-oscillator.

ENDOR frequencies were measured, with and without stress applied to the sample, as a function of the magnetic field within the range of the EPR linewidth. As explained in previous work,[3] special care was taken to avoid or compensate unwanted experimental effects arising from the shifts of the EPR lines with stress.

B. Ligand-ENDOR Hamiltonian

The lowest-energy multiplet of Tm^{2+} ions is $(4f^{13}, {}^2F_{7/2})$ which is crystal field split in cubic symmetry into two doublets Γ_6 and Γ_7, and a quartet Γ_8. In CaF_2, SrF_2, and BaF_2, the Γ_7 doublet is the ground state and the EPR spectrum consists of two isotropic lines, described by the spin Hamiltonian

$$H=g\mu_B\vec{H}\cdot\vec{S}+A\vec{S}\cdot\vec{I}\ , \tag{1}$$

where $S=\frac{1}{2}$ is the effective electronic spin of the doublet and $I=\frac{1}{2}$ is the nuclear spin of the 100% abundant ^{169}Tm isotope. The ENDOR Hamiltonian for the interaction with the nuclear spin of the neighboring $^{19}F^-$ ions is usually written

$$H_{\text{ENDOR}}=g_F\mu_n\vec{H}\cdot\vec{I}^F+A_p(3S_zI_z^F-\vec{S}\cdot\vec{I}^F)+A_s\vec{S}\cdot\vec{I}^F\ . \tag{2}$$

The first term is the Zeeman nuclear interaction between the external magnetic field H and the fluorine nuclear spin $I^F=\frac{1}{2}$, and the remaining two terms describe the transferred hyperfine interaction, with the z axis directed along the bonding axis.

In this experiment the uniaxial external stress was applied parallel to the crystallographic direction [111], and only the spectral ENDOR lines corresponding to the two nearest fluorine ions along this direction were measured. Their ENDOR frequencies, in the absence of external stress, are given by

$$h\nu_{\pm}=g_F\mu_nH+M(A_s-A_p)\ , \tag{3}$$

where $M=\pm\frac{1}{2}$ correspond to the quantum states of the electronic effective spin S. The change with stress of A_s-A_p was determined using this equation and the ENDOR frequency shifts measured for the center of the EPR lines. The results obtained for CaF_2 and SrF_2 are displayed in Table I, together with previous data on BaF_2.[3]

TABLE I. Change of the superhyperfine constants with uniaxial stress parallel to the [111] direction, $\partial(A_p - A_s)/\partial P$, in units of kHz kg^{-1} mm^2.

	Tm^{2+}:CaF_2	Tm^{2+}:SrF_2	Tm^{2+}:BaF_2
Experimental	−4.3(4)	−4.2(3)	−12.5(2)[a]
Calculated for undistorted lattice	−1.5	−2.1	−3.9
Calculated from Ref. 5	−1.1	−3.0	−12.9
Calculated this work	−2.1	−4.3	−9.9

[a]Reference 3.

C. Analysis of data

An important contribution to the superhyperfine parameter A_p is the dipole-dipole magnetic interaction $A_d = g g_F \mu_B \mu_n / R^3$. The remaining part $A_p - A_d$, as well as A_s, are of covalent origin and arise mainly from admixture of the impurity $4f$ wave function with the $2s$ and $2p$ wave functions of the fluorine ligands.[10] These parameters are dependent, in a first approximation, on the Tm^{2+} ion-fluorine ligand distance R and also on the electronic g value, through the dipole-dipole contribution to A_d. The stress derivative of the measured quantity $A_s - A_p$ is then given by

$$\frac{\partial(A_p - A_s)}{\partial P} = \frac{A_d}{g}\frac{\partial g}{\partial P} - \frac{3A_d}{R}\frac{\partial R}{\partial P} + \frac{\partial(A_p - A_d)}{\partial R}\frac{\partial R}{\partial P} - \frac{\partial A_s}{\partial R}\frac{\partial R}{\partial P} . \quad (4)$$

The first two terms are the partial derivatives of A_d, where $\partial g/\partial P$ is the stress-induced electronic g shift which is associated with the admixture of the Γ_7 ground-state wave functions with those of the excited Γ_8 quartet.[2,3] These shifts have been measured again in this experiment simultaneously with the ENDOR measurements and the excellent agreement found with previous results is taken as an indication of the proper alignment of the sample and the applied stress with respect to the magnetic field. In the last two terms of Eq. (4), $\partial A_s/\partial R$ and $\partial(A_p - A_d)/\partial R$ are estimated from the dependence of the measured values[7,11,12] of A_s and $A_p - A_d(R)$ with the actual $Tm^{2+} \rightarrow F^-$ distance R for the three fluorites MF_2 (M=Ca, Sr, Ba).

For the change $\partial R/\partial P$ in a perfect lattice, the classical theory of elasticity (homogeneous strain) gives

$$\frac{\partial R}{\partial P} = R(S_{11} + 2S_{12} + S_{44})/3 ,$$

where the S_{ij} are the elastic constants of the bulk. For fluorite lattices there is an additional displacement of the fluorine ions, that can be visualized as a relative movement of the two fluorine sublattices in the unit cell (see Fig. 1) whose origin is the electric field induced at the fluorine sites due to their lack of inversion symmetry.[2,3,6]

For the region around the impurity the values of R and $\partial R/\partial P$ are not those of the perfect lattice, due to the local distortions arising from the presence of the impurity. Values for R were calculated for Tm^{2+} by Anderson *et al.*[7] from ligand-ENDOR data, assuming[13] that $A_p - A_d(R)$ is proportional to A_s, and are given in Table II. Ivanenko and Malkin[6] have made an independent estimation for R (and $\partial R/\partial P$) by minimizing the local contributions to the cohesion energy and using *ab initio* calculated force constants[5] for the thulium-fluorine interaction. Their results for R, see Table II, agree with Anderson's for SrF_2 and BaF_2, where both models predict a lattice contraction of about 2% and 7%, respectively. In the case of CaF_2, however, Anderson *et al.*[7] give an expansion of 2% while Ivanenko and Malkin[6] have

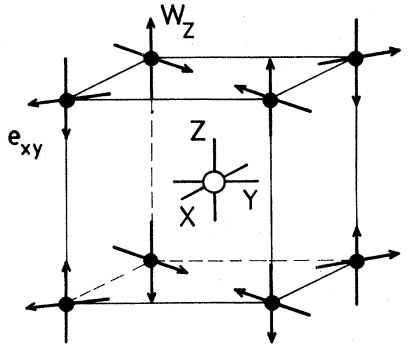

FIG. 1. Displacements W_z of fluorine ions (solid circles) around a metal site (open circle) for a macroscopic strain e_{xy}.

TABLE II. Impurity-ligand distance for Tm^{2+} in CaF_2, SrF_2, and BaF_2 (in Å units).

	CaF_2	SrF_2	BaF_2
Nearest neighbors			
Host[a]	2.3584[a]	2.5031[a]	2.6755[a]
Malkin *et al.*[b]	2.340	2.445	2.481
Anderson *et al.*[c]	2.400	2.446	2.499
This work	2.395	2.447	2.494
Next-nearest neighbors			
Host[a]	4.516[a]	4.793[a]	5.123[a]
Malkin *et al.*[b]	4.515	4.789	5.111
From superhyperfine data[d]	4.522	4.789	
This work	4.521	4.787	5.106

[a]Calculated from lattice parameters given in Table III.
[b]Reference 6.
[c]Calculated as in Ref. 7 with lattice parameters appropriate for 4.2 K.
[d]References 11 and 12.

calculated a contraction of 1%.

We have calculated Eq. (4) with Ivanenko and Malkin's values of R and $\partial R/\partial P$ for the three fluorite lattices with Tm^{2+} impurities[6] and the results are given in Table I. The importance of the local distortion can be appreciated by comparing these results with the values obtained using data corresponding to the host lattice. Comparing now both sets of results with the experimental data, a close agreement is found for SrF_2 and BaF_2 when including the effects of the local distortions. In the case of CaF_2 no improvement was obtained, and we believe this fact is related to the discrepancy already mentioned regarding the sign of the distortion for Tm^{2+} in CaF_2. The above arguments led us to develop an improved model for the local distortions in order to obtain a more consistent description of the results of ligand-ENDOR[7] and ligand–ENDOR-stress experiments for the three fluorides studied. A detailed description of the model is given in Sec. III.

III. LATTICE DISTORTIONS

A. Shell-model equations

The fluorite lattice MF_2 consists of three interpenetrated fcc lattices, one of divalent positive ions M^{2+} and two of nonequivalent negative fluorine ions, each with a lattice spacing a. As shown in Fig. 1, in this structure the metal ions are surrounded by eight fluorines at a distance $r_0'=\sqrt{3}a/4$ with equivalent F^- ions of the same sublattice occupying alternate corners of a regular cube. Each fluorine is in turn surrounded by six others in octahedral arrangement at a distance $r_0=a/2$. In this lattice the cohesion energy per formula unit $E_{\rm tot}$ has three contributions[14]:

$$E_{\rm tot}=\tfrac{1}{2}\alpha_M Z_M Z_F(e^2/r)+8\phi_1(r')+6\phi_2(r)\ . \tag{5}$$

The first term is the Coulomb energy, where $\alpha_M=5.8183$, is the Madelung constant, and $Z_M\,|e|$, $Z_F\,|e|$ are the net charges of the M^{2+} and F^- ions, respectively. The remaining two terms represent the short-range interaction between the metal ions and their nearest fluorines $\phi_1(r')$, and between neighboring fluorines $\phi_2(r)$.

When a metal ion is replaced by an impurity there is a change in the local contribution to the cohesion energy which is minimized through the relaxation of the nearest ions to new equilibrium positions and the induction of electrical dipoles on them. We have calculated this effect within the framework of the shell model,[14] where ions are described by a core which includes the nucleus and the inner electrons, with total charge $X\,|e|$, and an electron cloud idealized as a massless rigid spherical shell of charge $Y\,|e|$ as shown in Fig. 2. The sum $(X+Y)\,|e|$ is taken to be equal to the net ionic charge $Z\,|e|$.

The energy change $\Delta E_{\rm tot}$ for the distorted lattice is given by corresponding changes in the Coulomb energy ΔE_c and in the short-range interaction ΔE_r,

and there is also a contribution E_s associated with the formation of induced dipoles. In order to calculate these contributions we have assumed that the local cubic symmetry of the impurity site is maintained as it is shown by the EPR spectra, thus allowing only radial displacements of the ligands.

The change in the short-range interaction was calculated by expanding $\phi_1(r')$ and $\phi_2(r)$ about the equilibrium positions in the perfect lattice. For simplicity we have limited this expansion to second order in the displacements of the shells on the first four coordination spheres around the impurity (in the shell model short-range forces are assumed to act only between shells). We obtain

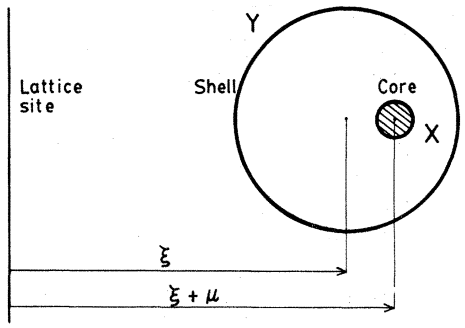

FIG. 2. Displaced equilibrium positions for the shell and core of ions in the vicinity of an impurity.

$$\Delta E_r/(e^2/a)=4\sqrt{3}(B_1^*-B_1)\xi_1+8(A_1^*-A_1)\xi_1^2+\tfrac{16}{3}(A_1+2B_1)(2\xi_1^2+6\xi_2^2+6\xi_3^2+3\xi_4^2-\sqrt{6}\xi_1\xi_2)$$
$$+(8/\sqrt{11})(3A_2+2B_2)(\sqrt{11}\xi_1^2-2\sqrt{3}\xi_1\xi_3)+(576/11)(A_2+B_2)\xi_3^2-(384/\sqrt{22})B_1\xi_2\xi_3$$
$$-(16/\sqrt{11})(A_1+8B_1)\xi_3\xi_4\,, \tag{6}$$

where ξ_i is the displacement of the center of the shell for the ions belonging to the ith coordination sphere, measured in units of the lattice constant a. The parameters B_1, A_1 and B_2, A_2 are the first and second derivatives of $\phi_1(r')$ and $\phi_2(r)$ evaluated at the equilibrium distances of the host lattice r_0 and r_0':

$$B_1=\frac{2v}{e^2}\left|\frac{1}{r'}\frac{\partial\phi_1(r')}{\partial r'}\right|_{r'=r_0'},\quad A_1=\frac{2v}{e^2}\left|\frac{\partial^2\phi_1(r')}{\partial r'^2}\right|_{r'=r_0'},$$
$$B_2=\frac{2v}{e^2}\left|\frac{1}{r}\frac{\partial\phi_2(r)}{\partial r}\right|_{r=r_0},\quad A_2=\frac{2v}{e^2}\left|\frac{\partial^2\phi_2(r)}{\partial r^2}\right|_{r=r_0}, \tag{7}$$

with $v=2r_0^3$ being the unit-cell volume; B_1^* and A_1^* have a similar expression and correspond to the first and second derivatives of the impurity-fluorine short-range interaction, also evaluated at r_0'.

The electrostatic contribution ΔE_c arises from the interaction between the displaced charges among themselves and with the induced electronic dipoles, as well as the interaction among these dipoles. This is given, in terms of the displacements ξ_i and μ_i (see Fig. 2), by

$$\Delta E_c/(e^2/a)=\sum_{i,j}h_{ij}(Z_i\xi_i+X_i\mu_i)\times(Z_j\xi_j+X_j\mu_j)\,, \tag{8}$$

where the charges Z_i (Z_j) and X_i (X_j) refer to the ions and cores, respectively, on the ith (jth) coordination sphere.

The numerical coefficients h_{ij} are related to the f_{ij} defined in Ref. 5, Eq. (6), by $h_{ij}=4f_{ij}/(Z_iZ_j)$; the values given below include corrections to some minor errors we found on the f_{ij}:

$$h_{11}=196.884\,,\quad h_{12}=73.786\,,$$
$$h_{13}=45.819\,,\quad h_{14}=11.340\,,$$
$$h_{22}=129.957\,,\quad h_{23}=400.189\,,$$
$$h_{24}=38.819\,,\quad h_{33}=518.061\,,$$
$$h_{34}=129.517\,,\quad h_{44}=7.114\,.$$

Finally, the energy associated with the formation of the electric dipoles

$$\vec{\mathrm{D}}_{i,g}=-Y_i\,|\,e\,|\,\mu_i a\vec{\mathrm{R}}_{i,g}/|\,\vec{\mathrm{R}}_{i,g}\,|$$

is given by

$$E_s/(e^2/a)=\sum_i N_i\mu_i^2a^3/(2\alpha_i/Y_i^2)\,, \tag{9}$$

where α_i is the core-centered polarizability of the ions on the ith coordination sphere and the subscript g identifies the different ions in the same

sphere, N_i being their total number.

The other related question of interest in this problem is the determination of the impurity-ligand displacement due to macroscopic strains. In our experiment, isotropic (Γ_1) and trigonal (Γ_5) strains were induced and these two cases are here analyzed.

For an isotropic stress we define, following Malkin's notation,[6] a local strain $e_i(\Gamma_1)$ for the case of the ions on the ith coordination sphere around the impurity. Here Γ_1 indicates the linear combination of components of the strain tensor that transforms like the Γ_1 irreducible representation of the O_h point symmetry group. Values for $e_i(\Gamma_1)$ were calculated by minimizing the total cohesion energy of the stressed lattice assuming that for $i>4$ the strain is homogeneous and equal to that of the perfect lattice.

The resulting equations were found to be formally equal to Eqs. (6), (8), and (9), if the following substitutions are made.

(i) $\xi_i a \rightarrow R_{i,g}[e(\Gamma_1)_i - e(\Gamma_1)]$, where $R_{i,g}e(\Gamma_1)$ is the radial displacement of the shell for the ions on the ith coordination sphere for the perfect lattice, and $R_{i,g}e(\Gamma_1)_i$ is the corresponding value around the impurity site.

(ii) $\mu_i \rightarrow \eta(\Gamma_1)_i$, where

$$\vec{d}(\Gamma_1)_{i,g} = -Y_i \mid e \mid \eta(\Gamma_1)_i a \vec{R}_{i,g} / \mid \vec{R}_{i,g} \mid$$

is an additional contribution to the electronic dipole moment of the ions on the ith coordination sphere due to the external stress.

(iii) $(B_1^* - B_1) \rightarrow (A_1^* - A_1)e(\Gamma_1)$.

For strains of trigonal symmetry, $e_i(\Gamma_5,\alpha)$ components are defined and calculated in a similar way as for the isotropic case. The fluorine ions occupy sites lacking inversion symmetry and for this reason an electric field proportional to the applied stress is induced, which polarizes the fluorine ions and also produces a displacement $2W$ of one fluorine sublattice with respect to the other.[2,6] In particular, when only a macroscopic e_{xy} strain is induced in the crystal, both the induced dipole moment $d(\Gamma_5)_\nu$ and the displacement W_ν (for the shell) are parallel to the z axis, as schematically shown in Fig. 1. These quantities are given by

$$\begin{aligned}
&\vec{W}_\nu = \tfrac{1}{4}\epsilon_\nu a\omega\hat{z} \ , \\
&\omega = \frac{\frac{1}{3}(B_1 - A_1) - 5.0288 Z_M Z_F}{\frac{1}{3}(A_1 + 2B_1) + (A_2 + 2B_2)} e_{xy} \ , \\
&\vec{d}(\Gamma_5)_\nu = -\tfrac{1}{4}\epsilon_\nu Y_F \mid e \mid \eta(\Gamma_5) a\hat{z} \ , \\
&\eta(\Gamma_5) = -40.2304 Z_M \frac{X_F \alpha_F}{Y_F^2 a^3} e_{xy} \ ,
\end{aligned} \tag{10}$$

where $\epsilon_\nu = \pm 1$ for $\nu = 1,2$ labeling the two fluorine sublattices.

The local strains in the distorted lattice were calculated by minimizing the following expression for the energy:

$$\Delta E(\Gamma_5) = \Delta E_r + \Delta E_{d1} + \Delta E_{dd} + \Delta E_s \ ,$$

where the different contributions are given by the following.

(i) The change in short-range interaction ΔE_r,

$$\begin{aligned}
\Delta E_r/(e^2/a) = &[\tfrac{3}{2}A_2 + 3B_2 + \tfrac{2}{3}(A_1 + 2B_1) + \tfrac{1}{6}(A_1^* - A_1) + \tfrac{1}{3}(B_1^* - B_1)]\omega_s^2 \\
&+ \tfrac{1}{4}[A_2 + 4B_2 + \tfrac{4}{3}(A_1 + 2B_1)](e_s - e_{xy})^2 + (A_2 + 2B_2)\omega\omega_s \\
&+ \tfrac{1}{12}[2(A_1^* - A_1) + (B_1^* - B_1)]e_s^2 - \tfrac{4}{3}(B_1 - A_1)\omega_s e_{xy} - \tfrac{1}{3}[(B_1^* - B_1) - (A_1^* - A_1)]\omega_s e_s \ ,
\end{aligned} \tag{11}$$

where e_s and ω_s are the displacements (in units of $a/4$) of the shells for the fluorines at $R_{1,g}(x_g, y_g, z_g)$, parallel to the $\hat{n}_g$ and $\hat{z}$ directions, respectively, with

$$\hat{n}_g = \frac{x_g\hat{y} + y_g\hat{x}}{(x_g^2 + y_g^2)^{1/2}} \ .$$

(ii) The interaction between the dipole moments and the resultant electric field of the lattice ΔE_{dl},

$$\Delta E_{dl}/(e^2/a) = 40.2304(Y_F\omega_s + X_F\omega_c)e_{xy} \ , \tag{12}$$

where ω_c is the z shift of the core (in units of $a/4$) of the fluorine ions.

(iii) The dipole-dipole contribution,

$$\Delta E_{dd}/(e^2/a)=\left[\frac{\sqrt{2}}{8}+\frac{\sqrt{3}}{9}-2\right][Y_F(e_s-e_{xy})+X_F(e_c-e_{xy}]^2$$
$$+\left[\frac{4\sqrt{3}}{9}-\frac{3\sqrt{2}}{2}\right][Y_F(e_s-e_{xy})+X_F(e_c-e_{xy})]\{Y_F(\omega_s-\omega)+X_F[\omega_c-\omega-\eta(\Gamma_5)]\}\ , \quad (13)$$

where ω and $\eta(\Gamma_5)$ are given by Eq. (10), and e_c is the displacement of the core of the nearest fluorines, in units of $a/4$ and in the direction of $\hat{n}_g$.

(iv) Finally, the induced dipoles,

$$\vec{d}(\Gamma_5)_{1,\nu}=-Y_F\,|\,e\,|\,a\left[\frac{\sqrt{2}}{2}\eta(\Gamma_5)_{n_g}\hat{n}_g+\epsilon_\nu\eta(\Gamma_5)_z\hat{z}\right]e_{xy}\ ,$$

where $\eta(\Gamma_5)_z=\frac{1}{4}(\omega_c-\omega_s)e_{xy}$ and $\eta(\Gamma_5)_{n_g}=\frac{1}{4(e_c}-e_s)e_{xy}$, give rise to the change in E_s:

$$\frac{\Delta E_s}{e^2/a}=\frac{Y_F^2}{8\alpha_F/a^3}[2(\omega_c-\omega_s)^2+(e_c-e_s)^2]\ . \quad (14)$$

B. Parameter evaluations

The short-range parameters B_1, A_1, and B_2, A_2 have been evaluated by Axe[14] for CaF_2, SrF_2, and BaF_2 from the elastic constants of these lattices. Here we have recalculated them using more recent and accurate low-temperature data for the elastic constants and lattice parameters, shown in Table III.

Figure 3 shows the dependence of B_2 with the fluorine-fluorine distance for different fluorites, and the change of sign observed in going from SrF_2 to BaF_2 indicates that the interaction changes from repulsive to attractive in that range. Owing to the simple power-law dependence assumed[14] for $\phi_2(r)$, the calculated second-derivative parameter A_2 also changes sign for BaF_2. However, the competition between attractive and repulsive forces in this region may lead to deviations from a single power-law dependence for the resulting interactions, as suggested by the r_0 dependence of B_2 in Fig. 3. For this reason we have considered a better approach to estimate A_2 for BaF_2 from Fig. 3, and this is the value we show in parentheses in Table III.

In order to evaluate the parameters describing the short-range interaction between the impurity Tm^{2+} and the fluorine ligands A_1^* and B_1^* we followed a different procedure since TmF_2 does not exist.[15] We have considered a hypothetical compound "TmF_2" with a lattice constant $a=5.61$ Å, interpolated (see Fig. 4) from crystallographic data of other difluorides known to have fluorite structure.[16–18] This value of the TmF_2 lattice parameter was then used to interpolate a value for B_2, in Fig. 3, which, together with the equilibrium condition[14]

$$B_1+B_2-\tfrac{1}{3}Z_MZ_F\alpha_M=0 \quad (15)$$

obtained by minimizing Eq. (5) with respect to r, yielded a value for B_1. Here B_1 is proportional to the first derivative of the thulium-fluorine short-range interaction evaluated at the equilibrium distance of TmF_2. Values for the first and second derivatives B_1^* and A_1^* evaluated at the equilibrium distance of the different host lattices were obtained assuming $\phi_1 \propto R^{-n}$. The compound EuF_2 is the only rare-earth difluoride whose elastic constants are presently known, thus allowing a calculation of the exponent n. We have taken this value to be the same for TmF_2 since n does not change much for different fluorides, as seen in Table III. All the short-range parameters as well as the charge of the shells and cores and the electric polarizabilities we used are also given in Table III.

C. Results

Our results for the equilibrium distance to the first and second fluorine neighbors for Tm^{2+} in CaF_2, SrF_2, and BaF_2 are given in Table II and show a remarkably good agreement with the values derived from ligand-ENDOR measurements.[7,10] As a further test to our model we have calculated the local distortion for Eu^{2+} in the same lattices, as shown in Table IV. Again good agreement was found when comparing our results with the values obtained from ENDOR data,[10,13,20] and also from the correlations between the measured crystal-field parameters in the three lattices and their dependence on hydrostatic pressure.[19,20]

Finally, in Table V we give our calculated values

TABLE III. Quantities used in the calculations of the lattice distortions, at 4 K.

	CaF_2	SrF_2	BaF_2	EuF_2
a (Å)	5.4465[a]	5.7808[b]	6.1787[b]	5.778[b]
c_{11} (10^{11} dyn cm^{-2})	17.124[c]	12.87[d]	9.810[e]	12.40[f]
c_{12} (10^{11} dyn cm^{-2})	4.675[c]	4.748[d]	4.481[e]	5.08[f]
c_{44} (10^{11} dyn cm^{-2})	3.624[c]	3.308[d]	2.544[e]	3.18[f]
$(e^2/2v)$ (10^4 dyn cm^{-1})	0.2856	0.2388	0.1956	0.2391
A_1	30.536	34.213	38.069	35.298
B_1	−3.632	−3.817	−3.971	−3.907
n_1	7.41	7.96	8.59	8.035
A_2	2.469	0.619	−0.645 (0.30)[g]	−0.281
B_2	−0.247	−0.062	0.092	0.028
n_2[i]	9	9	6	9
α_F (Å^3)[h]	0.74	0.77	0.87	
X_F[i]	1.35	1.35	1.35	
X_F[i]	−2.35	−2.35	−2.35	
α_M (Å^3)[h]	1.01	1.50	2.18	
X_M[i]	10.7	11.9	13.3	
Y_M[i]	−8.7	−9.9	−11.3	
$Tm^{2+}A_1^*$	40.97	26.34	16.80	
B_1^*	−4.52	−2.92	−1.86	
$Eu^{2+}A_1^*$	53.49	35.18	22.02	
B_1^*	−5.92	−3.89	−2.44	

[a]D. N. Batchelder and R. O. Simmons, J. Chem. Phys. 41, 2324 (1964). Value measured at 6.4 K.
[b]Reference 16.
[c]Extrapolated to 4 K from P. S. Ho and A. L. Ruoff, Phys. Rev. 161, 864 (1967).
[d]D. Gerlich, Phys. Rev. 136, A1366 (1964).
[e]D. Gerlich, Phys. Rev. 135, A1331 (1964).
[f]D. H. Kuhner, H. V. Lauer, and W. E. Bron, Phys. Rev. B 5, 4112 (1972).
[g]Value obtained from Fig. 3, see Sec. III B.
[h]J. C. Sharma, H. P. Sharma, and Jai Shanker, J. Chem. Phys. 67, 3642 (1977).
[i]Reference 14.

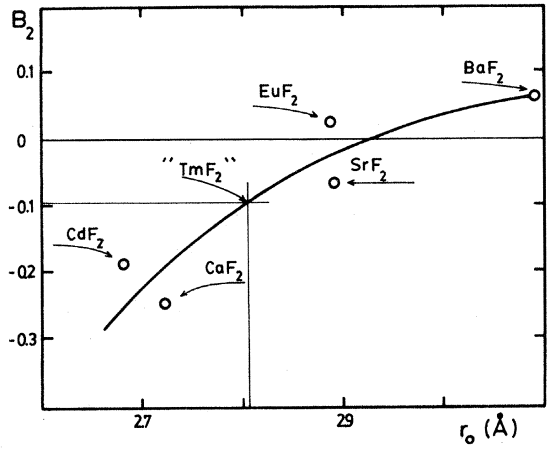

FIG. 3. First derivative coefficient for the $F^- \rightarrow F^-$ short-range interaction as a function of the interionic distance.

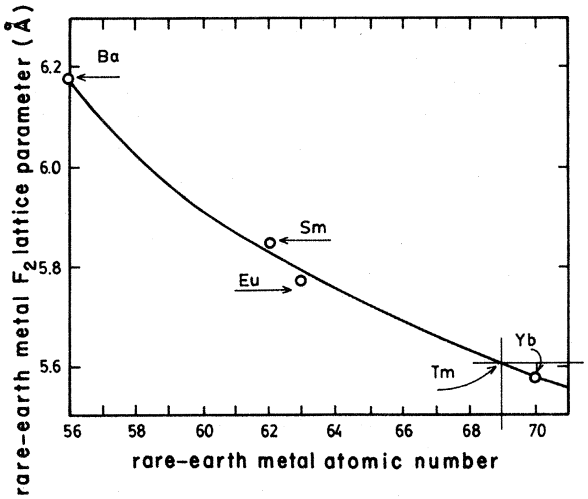

FIG. 4. Interpolation of a lattice parameter for TmF_2.

TABLE IV. Impurity-ligand distance for nearest and next-nearest fluorine ions for Eu^{2+} in CaF_2, SrF_2, and BaF_2 (in Å units).

	CaF_2	SrF_2	BaF_2
Nearest neighbors			
Host[a]	2.3584	2.5031	2.6755
Malkin *et al.*[b]	2.371	2.471	2.522
Baberschke[c]	2.443	2.502	2.583
From crystal-field parameters[d]	2.450	2.512	2.580
This work	2.436	2.507	2.565
Next-nearest neighbors			
Host[a]	4.516	4.793	5.123
Malkin *et al.*[b]	4.517	4.791	5.114
From superhyperfine data[e]	4.550	4.806	5.101
This work	4.527	4.794	5.110

[a]Calculated from lattice parameters given in Table III.
[b]Reference 6.
[c]Calculated as in Ref. 13 with lattice parameters appropriate for 4.2 K.
[d]Reference 20.
[e]References 10 and 20.

for the total strains and sublattice displacement for Tm^{2+} in the three lattices, where they can be compared with those obtained from Ref. 5. Both sets of values have been used in calculating the results of Table I.

IV. DISCUSSIONS

We have used the values of the impurity-ligand distance R and that of its change with stress $\partial R/\partial P$ calculated in Sec. III to evaluate the change with stress of the transferred hyperfine parameters from Eq. (4), and the results are given in Table I.

A detailed analysis of the contribution of each term in Eq. (4) shows that the difference between our results and those derived from Ivanenko and Malkin's model for the local distortions arises mainly from the R dependence of the covalent parameters in the last two terms.

This dependence is shown in Figs. 5(a) and 5(b) where we have also included for comparison the values obtained using the lattice parameter of the host. It is worth mentioning that when fitting the covalent parameters A_s and $A_p - A_d(R)$ to a power law R^{-n} with our calculated values for R, quite similar values for n are obtained in both cases: $n_s = 12.4$ (0.7) and $n_p = 12.3$ (1.3). This result supports the assumption of Anderson *et al.*[7] on the proportionality between the covalent parameters.

The consideration of local distortions around the impurity clearly provides a closer agreement with the experimental data than can be obtained from

TABLE V. Local strains for Tm^{2+} impurities in the fluorides.

	CaF_2	SrF_2	BaF_2
$e_1(\Gamma_1)/e(\Gamma_1)$	0.819	1.197	1.690
	(0.893)[a]	(0.943)	(1.351)
$e_1(\Gamma_5)/e(\Gamma_5)$	0.841	1.166	1.648
	(0.800)	(0.862)	(1.136)
$\omega_1/e(\Gamma_5)$	−0.301	−0.270	−0.125
	(−0.276)	(−0.317)	(−0.252)

[a]Values in parentheses are from Ref. 5.

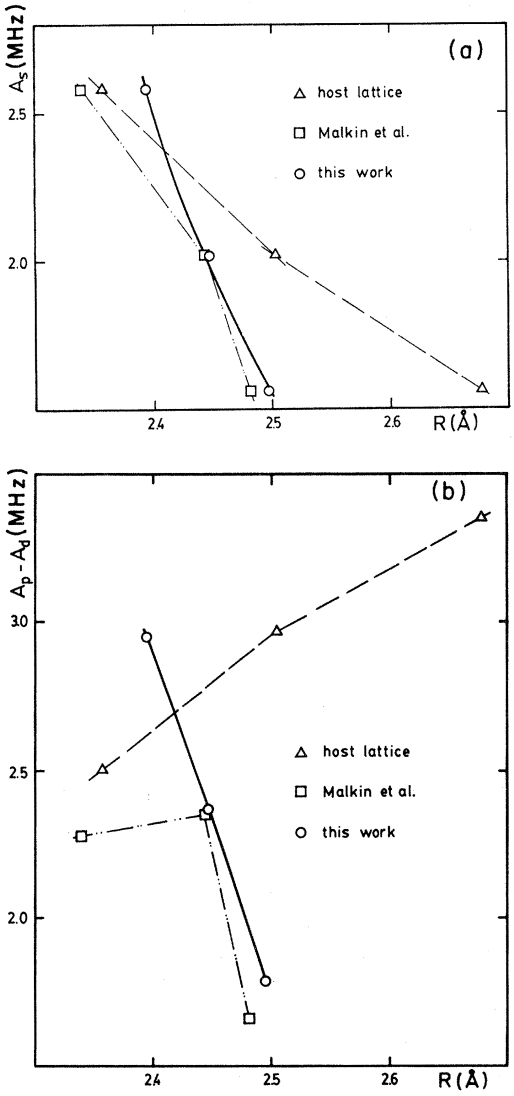

FIG. 5. (a) Dependence of the covalent parameter A_s on the impurity-ligand distance R from different models. Solid line indicates best fitting to $A_s \propto R^{-n_s}$ with $n_s = 12.4$ (0.7). (b) Dependence of the covalent parameter $[A_p - A_d(R)]$ on the impurity-ligand distance R from different models. Solid line indicates best fitting to $[A_p - A_d(R)] \propto R^{-n_p}$, with $n_p = 12.3$ (1.3).

the parameters of the host lattice. However, there still remain appreciable differences that cannot be further reduced within the framework of our model. Other mechanisms that could explain these differences arise from stress-induced changes in the wave functions that we have neglected in writing Eq. (4), when considering only an R dependence for the covalent contributions. First, the admixture of the Γ_8 wave functions into the Γ_7 ground state of Tm^{2+}, leads to a change in the transferred hyperfine parameters, whose order of magnitude we have estimated from the Baker and Fainstein[3] expression

$$\frac{\partial(A_p - A_d - A_s)}{\partial P} = \frac{A_p - A_d - A_s}{g} \frac{\partial g}{\partial P} .$$

This contribution amounts to less than 1% in all the cases we have considered in this work.

A second effect arises from the electrostatic polarization of the fluorine ions that is induced by both the local distortions and the externally applied stress. The mechanism of polarization is an admixture of $3s$ and $3p$ orbitals into the $2p$ and $2s$ wave functions of the fluorine ions that affects the covalent contribution to the transferred hyperfine interaction,[10,20] and hence the contribution of the last two terms to the evaluation of $\partial(A_p - A_s)/\partial P$. Moreover, the stress-induced polarization will give rise to an extra term in Eq. (4):

$$\frac{\partial(A_p - A_s)}{\partial d} \frac{\partial d}{\partial P} ,$$

where d is the induced electric dipole for stress applied along the [111] direction. The value of d can be derived from the parameters given in Table VI.

However, a numerical evaluation of these contributions is difficult due to the various assumptions involved in theoretical models[20] and the lack of sufficient experimental data. Work is in progress to measure separately the change of A_s and A_p with a Γ_3 stress, and to obtain similar data from the isoelectronic Yb^{3+} in CaF_2. Comparison of

TABLE VI. Stress-induced dipole moments for the first fluorine sphere of coordination around Tm^{2+} impurity.

	CaF_2	SrF_2	BaF_2
$10^3\eta(\Gamma_1)_1$	−3.02	2.94	9.65
$10^3\eta(\Gamma_5)_{ng}$	0.721	−0.663	−2.37
$10^3\eta(\Gamma_5)_z$	−22.40	−19.71	−18.54

Tm^{2+} and Yb^{3+} results in CaF_2 will be of interest due to the larger induced dipole by the trivalent rare earth, and because it will provide a further test to our model for the local distortions.

ACKNOWLEDGMENTS

We wish to thank Ing. Pedro Tadini for the electron irradiation of the samples in the LINAC facility, and Dr. C. E. Soliverez and Dr. M. Ahlers for critical reading of the manuscript. This work was supported in part by the International Atomic Energy Agency and the Consejo Nacional de Investigaciones Científicas y Técnicas (Argentina).

---

*Consejo Nacional de Investigaciones Científicas y Técnicas, República Argentina.
†Comisión Nacional de Energía Atómica.
‡Comisión Nacional de Energía Atómica and Universidad Nacional de Cuyo.

[1]E. R. Feher, Phys. Rev. 136, A145 (1964).
[2]J. M. Baker and D. van Ormondt, J. Phys. C 7, 2060 (1974).
[3]J. M. Baker and C. Fainstein, J. Phys. C 8, 3685 (1975).
[4]E. S. Sabisky and C. H. Anderson, Phys. Rev. B 1, 2028 (1970).
[5]B. Z. Malkin, Fiz. Tverd. Tela (Leningrad) 11, 1208 (1969) [Sov. Phys.—Solid State 11, 981 (1969)].
[6]Z. I. Ivanenko and B. Z. Malkin, Fiz. Tverd. Tela (Leningrad) 11, 1859 (1969) [Sov. Phys.—Solid State 11, 1498 (1970)].
[7]C. H. Anderson, P. Call, J. Stott, and W. Hayes, Phys. Rev. 11, 3305 (1975).
[8]C. Fainstein and C. Ramos, preliminary results presented at the ISMAR-Ampere International Conference on Magnetic Resonance, Delft, The Netherlands, 1980 (unpublished).
[9]C. Fainstein and S. B. Oseroff, Rev. Sci. Instrum. 42, 547 (1971).
[10]J. M. Baker, J. Phys. C 1, 1670 (1968); 10, 3323 (1977).
[11]R. G. Bessent and W. Hayes, Proc. R. Soc. London, Ser. A 285, 430 (1965).
[12]W. Hayes and P. H. S. Smith, J. Phys. C 4, 840 (1971).
[13]K. Baberschke, Phys. Lett. 34A, 41 (1971).
[14]J. D. Axe, Phys. Rev. 139, A1215 (1965).
[15]H. P. Beck, J. Solid State Chem. 23, 213 (1978).
[16]Calculated from the lattice constant at room temperature given by F. S. Galasso, in *Structure and Properties of Crystalline Solids,* International Series of Monographs in Solid State Physics, edited by N. Kurti and R. Smoluchowski (Pergamon, New York, 1970), Vol. 7, and the thermal expansivities given by A. C. Bailey and B. Yates, Proc. Phys. Soc. London 91, 390 (1967). For EuF_2 the same thermal expansivity as for CaF_2 was used.
[17]T. Petzel and O. Greis, J. Less-Common Met. 46, 197 (1976).
[18]J. J. Stezowski and H. A. Eick, Inorg. Chem. 9, 1102 (1970).
[19]W. R. Hurren, H. M. Nelson, E. G. Larson, and J. H. Gardner, Phys. Rev. 185, 624 (1969).
[20]J. M. Baker, J. Phys. C 12, 4039 (1979).